Journal of Chromatography A, 1218 (2011) 5263–5272

Contents lists available at ScienceDirect

Journal of Chromatography A

journal homepage: www.elsevier.com/locate/chroma

A study of mass transfer kinetics of alanyl-alanine on a chiral crown ether stationary phase

Leonid Asnin, Kavita Sharma, Se Won Park*

Department of Molecular Biotechnology, Konkuk University, 1 Hwayang-dong, Gwangjin-gu, Seoul 143-701, South Korea

ARTICLE INFO

Article history:
Received 1 March 2011
Received in revised form 2 June 2011
Accepted 7 June 2011
Available online 17 June 2011

Keywords:
Chiral chromatography
Alanyl-alanine
ChiroSil
Mass transfer kinetics

ABSTRACT

The mass transfer kinetics of alanyl-alanine enantiomers in a column packed with a chiral stationary phase (CSP) ChiroSil RCA(+) was studied by means of the moment method. Methanol–water solutions acidified with sulphuric acid were used as the mobile phase. It was shown that the spreading of peaks in the column was strongly affected by abnormal eddy diffusion. This effect was well described within the framework of the Giddings coupling theory. The comprehensive four-term Giddings equation for eddy diffusion was applied, considering simultaneous contribution of the trans-column, trans-channel, short-range inter-channel, and long-range inter-channel dispersion factors. Through these calculations, a predominant importance of the trans-column flow velocity bias was revealed. Besides eddy diffusion, the adsorption kinetic resistance to mass transfer plays a noticeable role in band broadening, all the other contributions (from longitudinal molecular diffusion, external and intraparticle mass transfer) being of minor significance. A relative importance of the mass transfer kinetics increases correlatively with a growth of the retention factor. Both the retention and kinetics of the adsorption of alanyl-alanine on the CSP in study are enantioselective. The influence of the column pressure on retention as well as corrections required because of this influence are also discussed.

1. Introduction

Enantioselective adsorption is a fundamental phenomenon involved in the separation of optical isomers by chiral chromatography. The last two decades have seen significant progress in this area [1], driven by needs of pharmaceutical, agrochemical, and fragrance industries [2,3]. Most researchers focused on the study of adsorption equilibrium whereas little attention was paid to the study of mass transfer kinetics in chiral columns. The majority of works devoted to this problem dealt with chiral stationary phases (CSPs) based on chiral macromolecules such as proteins [4,5], polysaccharides [6–10] or molecularly imprinted polymers (MIPs) [11–13]. There are few publications [14,15] devoted to brush-type CSPs. Unfortunately, there is almost no information about enantioselective mass transfer on the brush-type stationary phases with bonded macrocyclic ligands (cyclodextrins or chiral crown ethers) except the work of Ringo and Evans [16], who reported the HETP values of several chiral tracers eluted from a β-cyclodextrin CSP without a detailed investigation of mass transfer mechanisms.

The present work is aimed at the elaboration of the mass transfer kinetics of LL- and DD-alanine dimers on a ChiroSil RCA(+) CSP bearing a chiral crown ether as a selector (Fig. 1). Crown ethers bind to amino acids by the mechanism of host–guest complexation [17,18]. In this sense they are similar to polysaccharides and MIPs but distinctive from Pirkle and similar type selectors whose retention mechanism does not involve inclusion binding. On the other hand, crown ether CSPs retain positive properties of brush-type adsorbents in terms of accessibility of bound ligands to interaction with solutes (in polymeric phases chiral selectors are distributed in the polymer matrix therefore access to them can be hindered). It is of theoretical interest to investigate transport processes in a CSP with such "intermediate" properties. Ala-Ala was taken as a test adsorbate because its chromatographic behaviour on the CSP under consideration has been described and rationales to achieve an optimal enantioresolution have been given [19]. We followed these recommendations in the selection of experimental conditions for the present research.

There are three main approaches to the investigation of mass transfer processes in chromatography: the numerical simulation of band profiles using different dynamic models of chromatography [20], the stochastic analysis [21], and the moment method [20]. The latter technique was chosen in this study as providing detailed information about mass transfer processes. Its special advantage is that the method allows analysing the axial dispersion, which was found to be an important contributor to the peak broadening in the system of study.

* Corresponding author. Tel.: +82 2 3436 5439; fax: +82 2 3436 5439.
E-mail address: sewpark@konkuk.ac.kr (S.W. Park).

0021-9673/$ – see front matter © 2011 Elsevier B.V. All rights reserved.
doi:10.1016/j.chroma.2011.06.029

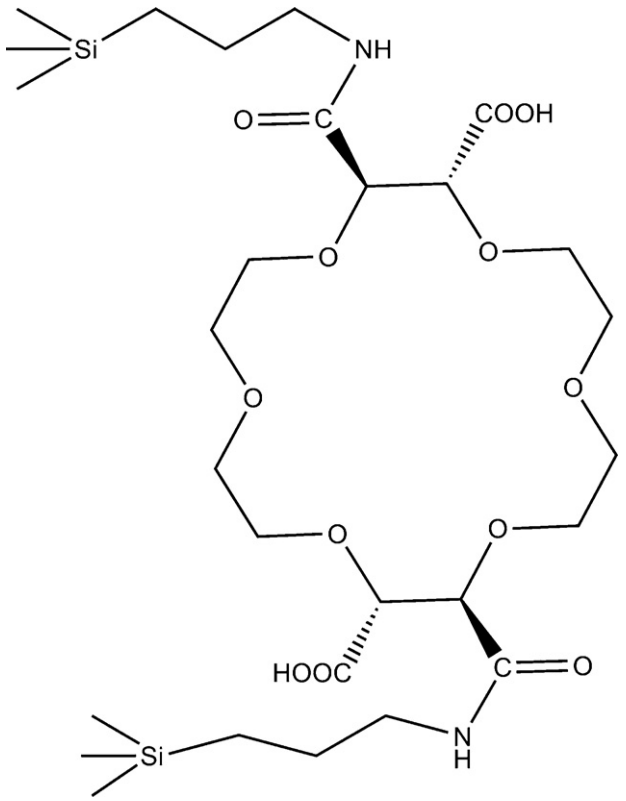

Fig. 1. Chemical structure of a ChiroSil RCA(+) chiral selector.

2. Theory

In chromatography, physico-chemical properties of an adsorption system can be derived from the first (μ_1) and the second central (μ_2') moments of an elution peak profile. By definition,

$$\mu_1 = \frac{\int c(t)t dt}{\int c(t)dt} \quad (1)$$

$$\mu_2' = \frac{\int c(t)(t-\mu_1)^2 dt}{\int c(t)dt} \quad (2)$$

where c is the solute concentration at the outlet of a column and t is time. For a system with a linear adsorption isotherm, the first moment relates to the adsorption equilibrium constant K as [20]

$$\mu_1 = \frac{L}{u\varepsilon_e}(\varepsilon_T + (1-\varepsilon_T)K) \quad (3)$$

In this expression, L is the column length, u the interstitial linear flow velocity, and ε_T the total void fraction of the column. It includes the interparticle void fraction ε_e and the particle (internal) porosity ε_i; $\varepsilon_T = \varepsilon_e + \varepsilon_i(1-\varepsilon_e)$.

The second central moment characterizes the dispersion of a chromatographic peak and according to the Martin and Synge plate model of chromatography [20] is equal to the product $\mu_1 N$, where N is the number of theoretical plates. The ratio (L/N) known as the height equivalent to the theoretical plate, HETP or H, is more convenient in theoretical consideration.

In general, peak dispersion depends on two factors: the kinetics of non-equilibrium processes in a column and the curvature of an adsorption isotherm. For strongly diluted samples corresponding to the linear part of an adsorption isotherm band broadening is accounted for only by transport phenomena: axial dispersion, external mass transfer, intraparticle diffusion, and the rate of adsorption/desorption. In the framework of the general rate (GR) model of chromatography [20] an additive effect of these processes is described by the following equation:

$$H = \frac{2D_{ax}}{u} + 2u\left(\frac{k_1}{1+k_1}\right)^2 \left[\delta_{ext} + \delta_{int} + \delta_{ads}\right] \quad (4)$$

with

$$\delta_{ext} = \frac{d_p}{6\beta_e k_e}; \quad \delta_{int} = \frac{d_p^2}{60\beta_e D_i}; \quad \delta_{ads} = \left(\frac{k_p}{1+k_p}\right)^2 \frac{1}{\beta_e k_{ads}} \quad (5)$$

$$\beta_e = \frac{1-\varepsilon_e}{\varepsilon_e} \quad (6)$$

$$k_1 = \beta_e(\varepsilon_i + (1-\varepsilon_i)K) \quad (7)$$

$$k_p = \frac{1-\varepsilon_i}{\varepsilon_i}K \quad (8)$$

where d_p is the particle diameter, k_e the external mass transfer coefficient, D_{ax} the axial dispersion coefficient, D_i the intraparticle diffusivity, and k_{ads} the adsorption rate constant.

Axial dispersion is a complex phenomenon depending on molecular diffusion and different dispersion mechanisms resulting from any sorts of inhomogeneity in a bed of adsorbent that are usually combined under the term “eddy dispersion”. It was comprehensively discussed by Giddings [22]. He considered five categories of flow inequalities contributing into the eddy dispersion on different length scales: trans-particle, trans-channel, short-range inter-channel, long-range inter-channel, and trans-column effects. The first source of velocity bias is included into the intraparticle diffusion mechanism in the GR model [23]. The rest four sources of spatial velocity fluctuations together with the longitudinal molecular diffusion compose the axial dispersion term of the plate equation, with γ standing for the obstructive factor and D_m being the molecular diffusivity:

$$H_{ax} = \frac{2D_{ax}}{u} = \frac{2\gamma D_m}{u} + \sum_{i=1}^{4} \frac{1}{1/(2\lambda_i d_p) + D_m/(\omega_i u d_p^2)} \quad (9)$$

The indices $i = 1, 2, 3, 4$ correspond to the trans-channel, short-range inter-channel, long-range inter-channel, and trans-column contributions to eddy dispersion, respectively. The coefficients ω and λ are universal structural parameters characteristic of each contribution. The first three pairs of the structural parameters were estimated by Giddings [22] to be $\omega_1 = 0.014$, $\lambda_1 = 0.5$; $\omega_2 = 0.5$, $\lambda_1 = 0.48$; $\omega_3 = 2$, $\lambda_3 = 0.1$. When obtained from the fitting of the experimental data to Eq. (9) under conditions allowing to neglect the trans-column contribution, those coefficients usually agree with Giddings’ estimation within an order of magnitude [23,24]. The Giddings’ estimation for the trans-column structure parameters $\omega_4 = 1060$ and $\lambda_4 = 85$ are too large, lacking physical meaning for today’s packed columns [25]. Gritti and Guiochon developed a theory predicting the extent of the trans-column eddy dispersion on the basis of the radial flow velocity profile [25]. They have shown that the trans-column contribution H_{tcol} for common reversed phase HPLC columns increases from nil to an asymptotic value ranging within an interval of $(2–4)d_p$ depending on bed properties and the retention of a tracer. It is smaller for retained solutes and larger for non-retained ones. The λ coefficient is around 1.5 and depends directly only on the shape of the flow velocity profile (which, in turn, is a function of bed properties). The ω coefficient is proportional to the factor $[1+k']^{-1}$ (k' is the retention factor), depending also on particle and bed dimensions and porosities, and on the flow velocity pattern. By an order of magnitude, it ranges between 10 and 100 for moderately retained solutes ($k' = 1–20$).

The combination of Eqs. (4) and (9) constitutes the Giddings HETP equation. It can be written in a form resembling the Van Deemter [26] equation:

$$H = A'(u) + \frac{2\gamma D_m}{u} + Cu \tag{10}$$

where the function $A'(u)$ represents the second term of the right hand side of Eq. (9) and the coefficient C is the Van Deemter kinetic parameter. It combines all the contributions to band broadening due to kinetic factors that are proportional to u. Deconvolving information concerning the individual kinetic processes from this coefficient is a task that is beyond the possibilities of chromatographic experiments. It must rely on some extra-chromatographic correlations. So, the external mass transfer coefficient is calculated using the Wilson–Geankoplis equation [27], which was proven to be valid for hydrodynamical conditions in common HPLC systems [14,28]:

$$k_e = 1.09\left(\frac{D_m}{d_p}\right)^{2/3} u^{1/3}\varepsilon_e^{-2/3} \tag{11}$$

The estimation of the intraparticle pore diffusivity is based on the model of Mackie and Mears [29] considering an adsorbent grain as a random network of uniformly sized pores. The final equation of this model reads

$$D_i = \left(\frac{\varepsilon_i}{2-\varepsilon_i}\right)^2 D_m \tag{12}$$

Identification of the intraparticle mass transfer with the pore diffusion implies the neglect of the surface diffusion. The latter effect is supposed to be important when the product $2[k_1/(1+k_1)]\delta_{\text{int}}$ is larger than an experimental C value. This would indicate that there is an additional diffusion flux reducing the intraparticle mass transfer resistance, which was not the case in the present work.

The molecular diffusivity of a solute can be found by means of the Wilke and Chang equation [30]:

$$D_m = 7.4\times 10^{-8}\frac{(\overline{\phi M})^{0.5}T}{\eta V_b^{0.6}} \tag{13}$$

where T is the absolute temperature, η the viscosity of the mobile phase. $(\overline{\phi M}) = \sum_i x_i\phi_i M_i$ (i = methanol, water) is a correction allowing for the influence of hydrogen bonding on molecular diffusion, x is the mole fraction of either solvent in the mixture, M_i the molecular mass of the mobile phase component i, ϕ the association coefficient, 1.9 and 2.6 for methanol and water respectively, and V_b is the molar volume of the solute at its boiling point. This last parameter was estimated with the help of the Le Bas increment method for Ala-Ala (182.5 cm^3/mole) and the Tyn and Calus method for toluene (118.7 cm^3/mole) as recommended in [30].

It must be noted that η is a function of pressure (P) due to a finite compressibility of the mobile phase. As pressure falls from the inlet to the outlet of the column, mobile phase viscosity will decrease in the same direction. In the calculation of molecular diffusivity, we used the value η reduced to the average pressure in the column. This is a sufficiently accurate approximation because the change of viscosity is minor within the range of pressures studied, less than 10% for the highest inlet pressure achieved (~300 bars). Both $\eta(P)$ and $D_m(P)$ functions are close to linear within the mentioned pressure interval. Empirical data on an $\eta(P)$ dependence needed for these calculations were found in the literature [31].

2.1. Plate height equation and the concept of a dual-site surface

The model of a dual-site surface is the central concept in studies of enantioselective adsorption [32]. This model is also valid in the given case as it was shown by the measurement of the adsorption isotherms of Ala-Ala enantiomers on a ChiroSil RCA CSP described in detail elsewhere [33]. The model assumes that a CSP bears two types of the adsorption sites, enantioselective and non-selective. The first group of sites associated with chiral selectors exhibits different affinity towards optical isomers whereas the adsorption sites belonging to the other group interact with optical antipodes identically. These two fundamental classes of adsorption sites can be composed of smaller groups of sites differing in affinity and/or kinetic properties [11,15]. We shall restrict the following consideration only to the simple dual-site model for the sake of simplicity. This concept is widely used in works devoted to the adsorption equilibrium in chiral systems [5,34–36] but is rare in mass transfer kinetics studies involving the technique of moment analysis. This is because of mathematical difficulties associated with the development of a respective plate height equation. So, Eq. (4) assumes homogeneous adsorption kinetics. Therefore adsorption rate constant k_{ads} is an apparent coefficient convoluting contributions from both types of the adsorption sites. Yamazaki derived a plate height equation for heterogeneous mass transfer kinetics after neglecting the contributions from the external and intraparticle mass transfer resistances [37]. Adopted to the dual-site model his treatment reveals the meaning of the apparent rate constant k_{ads}:

$$\frac{K^2}{k_{ads}} = \frac{\alpha_1 K_1^2}{k_{ads,1}} + \frac{\alpha_2 K_2^2}{k_{ads,2}} \tag{14}$$

where subscript indices 1 and 2 refer to adsorption sites of type 1 and 2, respectively, and symbols without the indices designate experimental apparent quantities. α_1 and α_2 are the relative surface densities of the adsorption sites of type 1 and 2, respectively. Note that $K = \alpha_1 K_1 + \alpha_2 K_2$.

Despite the fact that the required equilibrium characteristics of the adsorption system of interest are known [33], Eq. (14) cannot be used for the estimation of partial contributions to HETP from different adsorption sites without knowledge of the partial adsorption rate constants. These quantities can be derived from the analysis of overloaded band profiles by numerical methods [38,39]. This line of experimentation is currently undergoing further extensive investigation and results will be reported later. For purposes of the given work, the use of an apparent coefficient is sufficient.

3. Experimental

3.1. Equipment

The data were acquired using an Agilent 1100 liquid chromatograph (Agilent Technologies, Palo Alto, CA, USA) consisting of a binary pump, an auto-sampler, a column thermostat, a DAD detector, and a ChemStation data acquisition system. Chromatograms were recorded at the wavelength of 210 nm. The extra-column volume of the instrument was 0.051 ml as measured with a zero-volume connector in place of the column. All the retention data were corrected for this contribution. The column studied was ChiroSil RCA(+) from RStech (Daejeon, S. Korea), with dimensions 150 mm × 4.6 mm; particle size 5 μm, average pore size 100 Å.

The column void volume was determined using a Shimadzu (Kyoto, Japan) LC-VP series HPLC system equipped with a solvent delivery unit, a column thermostat, a refractive index detector, and a Rheodyne 7725i manual injector (Rheodyne, Cotati, CA, USA) with a 5 μl sample loop. The system was controlled by a computer station running the Class-VP software from Shimadzu.

3.2. Chemicals

For the preparation of the mobile phases, we used HPLC grade water from J.T. Baker (Phillipsburg, NJ, USA) and HPLC grade

methanol from Duksan (Seoul, S. Korea). Sulphuric acid (extra pure grade) was also supplied by Duksan. L-alanyl-L-alanine (99%) and D-alanyl-D-alanine (98%) were purchased from MP Biomedicals (Solon, OH, USA) and Sigma–Aldrich (St. Louis, MO, USA), respectively. Deuterated methanol (99.8%) used for hold-up volume measurements was from Alfa Aesar (Ward Hill, MA, USA). Toluene (ACS grade) was purchased from Sigma–Aldrich.

3.3. Procedures

The measurements of peak broadening were carried out at $25.0 \pm 0.2\,^{\circ}C$ in the flow rate range 0.1–2.0 ml/min by injections of 2 μl samples of DD- and LL-dipeptide. The concentration of the sample was 0.20 g/l. Each injection was repeated twice or until the two subsequent chromatograms coincided within 0.1% in terms of the retention time to ensure the establishment of equilibrium in the column. Measurements at each flow rate studied were repeated without the column to evaluate the effect of extra-column dispersion. All results were corrected for this contribution. The four water–methanol mobile phases modified with 5 mM H_2SO_4 were investigated, with the methanol percentage 60, 70, 80, and 90 vol.%. Eluents were degassed by sonication before use.

The void volume value was found by the isotopic method based on the retention of an isotopically labeled solute in the same but nonlabeled solvent [40]. Measurements were made at $25.0 \pm 0.2\,^{\circ}C$ using pure methanol as the mobile phase and deuterated methanol as the tracer. The tracer concentration was 1 vol.%, the sample size was 5 μl.

3.4. Calculations

3.4.1. Measurement of the plate height

The values of HETP were calculated from the first absolute moment and the second central moment of a chromatographic peak. The moments values were determined according to their definitions given in Eqs. (1) and (2). The integration was performed numerically using MathCad 14 software (PTC, Needham, MA, USA). Despite the method is straightforward and does not bring in the estimation of HETP any model bias, its practical implementation gives rise to several concerns. It is well known that the numerical integration of Eq. (2) using the raw data is strongly affected by random fluctuations of the detector signal, especially at the edges of band profiles [41–43]. To minimize the influence of interfering factors we performed integration between the points corresponding to 1% of the peak height. This cutoff level is higher than the signal noise amplitude. At the same time, it is low enough to include >99% of the peak area within the integration limits. Thus found HETP value will be designated below as H_μ.

The HETP was also estimated by means of the conventional half-height method. In this method, a peak is assumed to have a Gaussian shape that gives the known equation relating HETP, the retention time (t_R), and the peak width at half-height ($w_{0.5}$).

$$H_{0.5} = \frac{L}{5.545}\left(\frac{w_{0.5}}{t_R}\right)^2 \tag{15}$$

Unlike the H_μ quantity the value determined using the half-height method does not have a clear physical meaning in the case of unsymmetrical peaks. Nonetheless it is of interest to compare mass transfer coefficients derived from these two quantities to enlighten the effect of tailing on column efficiency, at least on empirical grounds.

3.4.2. Calculation of the plate height coefficients

The coefficients of the plate height equation were estimated by fitting the experimental data to a chosen equation using the Levenberg–Marquardt nonlinear regression algorithm as implemented in the Solver tool of Microsoft Excell 2007.

4. Results and discussions

4.1. Effect of the flow rate on retention

It is usually supposed that the retention factor does not depend on the flow rate. This is, however, a certain approximation. Because pumping the mobile phase requires applying pressure at the column inlet and because the mobile phase is compressible, the flow rate is not constant. It is a function of a local position in the column and its average value differs from the value measured at the column outlet at ambient temperature and pressure. The compressibility factor can be taken into account by integrating the local mobile phase density profile over the column. Indeed, the retention (in terms of the peak centroid) is [44]

$$\mu_1 = \int_0^L \frac{(\varepsilon_T/\varepsilon_e)}{u(z)}[1 + k']dz \tag{16}$$

where $u(z)$ is the local interstitial linear velocity at distance z from the column inlet. It is equal to $u(L)\cdot\rho(L)/\rho(z)$ according to the continuity equation (ρ is the mobile phase density). Given the pressure decreases from the inlet value P_{in} to the outlet value P_o linearly one can obtain

$$k' = \frac{\mu_1 u(L)\varepsilon_e}{\varepsilon_T}\left[\int_{P_o}^{P_{in}} \frac{\rho(P)}{\rho(P_o)}\frac{L}{(P_{in} - P_o)}dP\right]^{-1} - 1 \tag{17}$$

This equation provides values of the retention factor that are free from uncertainty imposed by the compressibility effect. All the retention data below were corrected correspondingly. In these calculations, we used a $\rho(P)$ function published in [31]. The magnitude of the correction factor did not exceed 1% at the highest flow rate studied.

Eq. (17) assumes that neither the total porosity nor the retention factor depend on pressure. This is an approximation too. In fact, k' is a function of pressure by requirements of thermodynamics [45,46].

$$\left[\frac{d(\ln\ k')}{dP}\right]_T = -\frac{\Delta V_m}{RT} + \frac{d(\ln\beta)}{dP} \tag{18}$$

ΔV_m is the change in partial molar volume of a solute upon adsorption, β is the phase ratio, and R is the gas constant. Depending on the sign of the ΔV_m, the k' value can increase or decrease with pressure and, consequently, with flow rate. Molar volume changes are usually small and positive for the adsorption on the chiral stationary phases [16,47,48]. According to data of [16,47,48] we can expect a decrease of retention by 2–10% for a 100-bar increase of pressure. Fig. 2 shows that it is not quite a case. The retention factors grow correlatively with the augmentation of back pressure to 140–150 bars (not for 90% methanol solution) followed by a decrease beyond this point. An extremum plot of the $k'[P_{in}(u)]$-function reveals the opposite influence of two effects. The one responsible for reduction in retention at high flow rates can be the thermodynamic effect described by Eq. (18). The other factor raising the k' values at low flow velocities is supposed to be of a non-thermodynamic origin. A progressive filling of small pores with the mobile phase as the pressure increases could cause the increasing branch of the $k' - u$ dependence. Indeed, as P_{in} increases corellatively with a growth of the flow rate, the mobile phase penetrates into narrow pores not occupied at lower pressures (if any) and the area of the liquid/solid interface is extending. It would result in an increase of the k' value. A somewhat different pattern observed with the 90:10 (v/v) methanol–water solvent can be explained by the dependence of the ΔV_m value and/or wettability of the mobile phase on its composition.

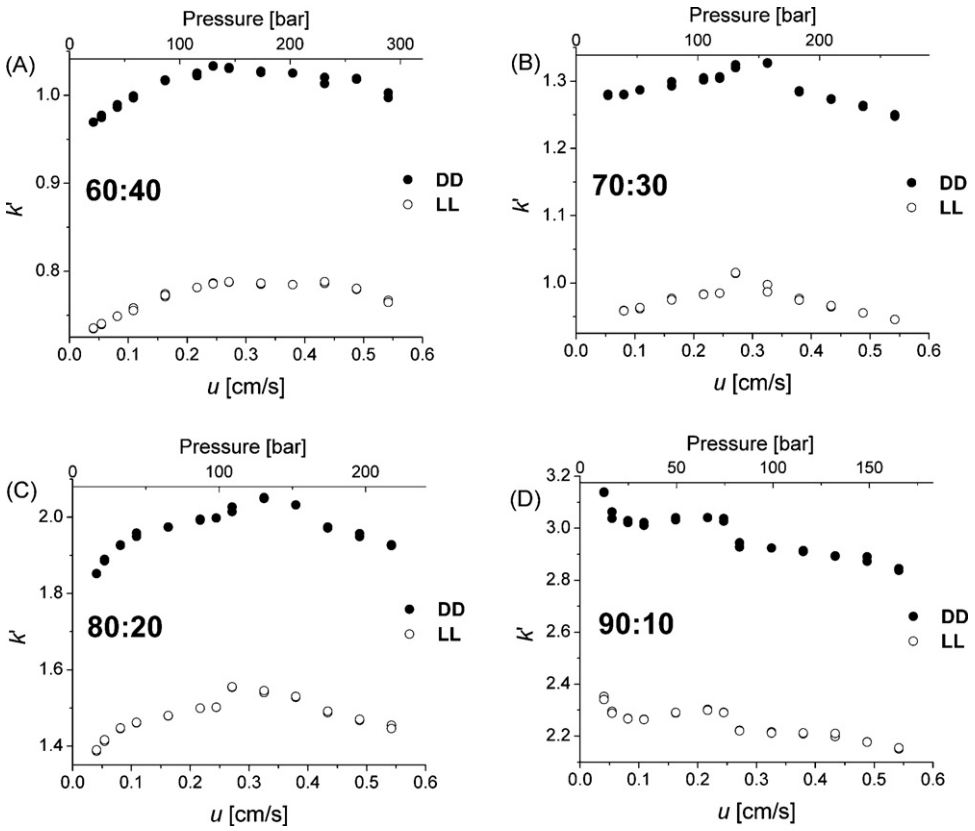

Fig. 2. Retention factor of D-Ala-D-Ala and L-Ala-L-Ala as a function of the linear flow velocity and the inlet pressure for mobile phases with different methanol–water ratio (shown on graphs).

4.2. Mass transfer kinetics

4.2.1. Peak shape

Peak shape is the primary source of information about adsorption processes in chromatography. Symmetrical peaks indicates the linear adsorption isotherm and supposedly fast adsorption/desorption kinetics. Unsymmetrical peaks, when linear conditions are proven, reveal slow mass transfer. A large tailing may indicate either slow desorption kinetics [5,38,39] or the irregularity of the packing structure across the column [49]. The shape of the peaks of Ala-Ala evolves from a quite symmetrical, close to Gaussian one at high flow velocities to unsymmetrical with a pronounce tail at low flow velocities (Fig. 3a). Note that the extent of tailing is rather similar for all the peaks shown in the figure. The symmetry of the profiles obtained at high flow velocities results from an even dispersion of the front and rear flanks of the peaks. It is not the case for the low flow velocity band profiles, where the front part is relatively sharp and the tail is dispersed. Observed tailing has a kinetic origin. A prove is given in Fig. 4 where chromatograms of D-Ala-D-Ala obtained after injection of samples with diminishing concentration at two different flow rates are shown. It is seen that neither the retention time shifts nor the shape of peaks changes as a function of sample size, indicating linear chromatography conditions. The asymmetry coefficient measured at 10% of the peak height (see Fig. 5a) was constant with the value 1.99 at a flow rate of 0.4 ml/min and fluctuated by ±7% around the value 1.61 at a flow rate of 1 ml/min.

The development of peak asymmetry involves the bottom part of the peaks. It is seen from Fig. 5 that asymmetry coefficients taken at the mid-height of peaks are close to 1 and does not depend on the flow rate. On the contrary, those coefficients measured at the 1 and 10% of the peak height rise significantly when the flow rate decreases. The figure shows data only for the mobile phase with 70% of methanol. The same pattern was found for all the other mobile phase compositions considered in this work. Fornstedt et al. have shown that such behaviour is specific to the dual-site surfaces with different mass transfer kinetics on each type of sites [38,39]. However injections of non-retained tracer (toluene) resulted in tailing peaks too (Fig. 3b) suggesting that the peak asymmetry originates in axial dispersion phenomena. On the other hand, toluene is eluted along with the system peak. It is not impossible that the latter would distort the toluene profile that would be symmetrical given the absence of the injection perturbation. Thus it is not clear what effect causes the peak tailing of the dipeptide, slow heterogeneous kinetics or axial dispersion, or both.

To exclude from consideration the effect of the extra-column dispersion, injection profiles at different flow rates were measured in the system without column. The resulting peaks were narrow, showing no pronounced tails. We also recorded chromatograms of toluene in a system with the column and an additional capillary (270 μl) attached to extend the extra-column volume. Two experiments were carried out, with the capillary attached before the column and with the capillary connected between the column and the detector. Chromatograms in both cases coincided. The tail was camouflaged by the overall peak broadening (Fig. 6). These results prove that the origin of the peak tailing resides in the bed of the stationary phase. The dispersion in the empty space would result in a rather symmetrical band broadening given the space is washed by the flow well.

4.2.2. Plate height equation

The plate equation written in a regular form (Eq. (10)) does not take into account the fact that the external mass transfer coeffi-

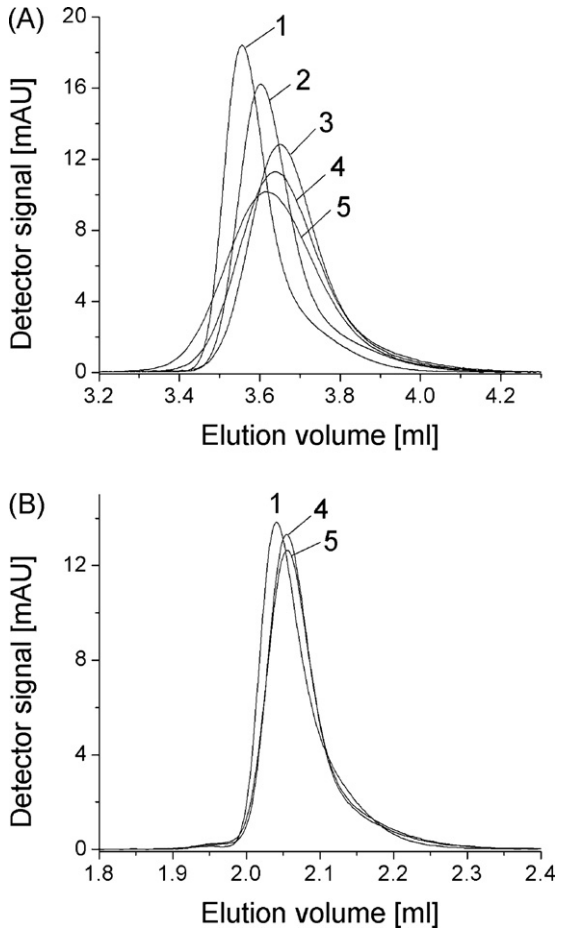

Fig. 3. Elution profiles of D-Ala-D-Ala (A) and toluene (B) at flow rate 0.2 ml/min (1), 0.40 ml/min (2), 0.90 ml/min (3), 1.4 ml/min (4), and 2.0 ml/min (5). Mobile phase: 5 mM H_2SO_4 in methanol–water (60:40, v/v).

cient is a function of u. It is more convenient for the sake of further analysis to rearrange this equation as follows.

$$H - H_{ext} = A'(u) + \frac{2\gamma D_m}{u} + C'u \tag{19}$$

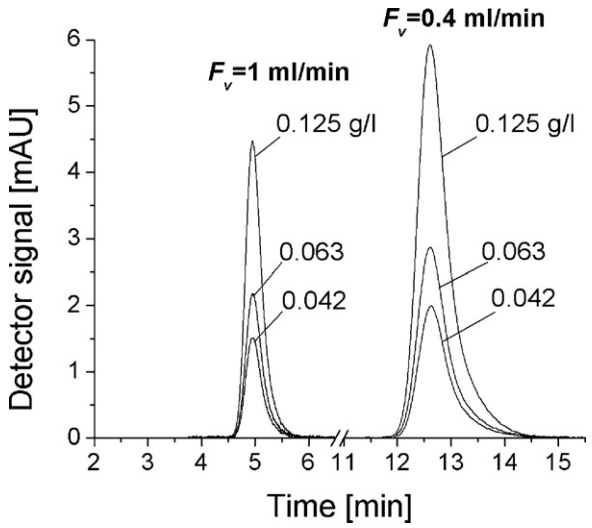

Fig. 4. Elution profiles of D-Ala-D-Ala for different sample concentrations (g/l; shown on graph) at flow rate (F_v) 0.4 and 1 ml/min. Sample volume 2 μl. Mobile phase: 5 mM H_2SO_4 in methanol–water (80:20, v/v).

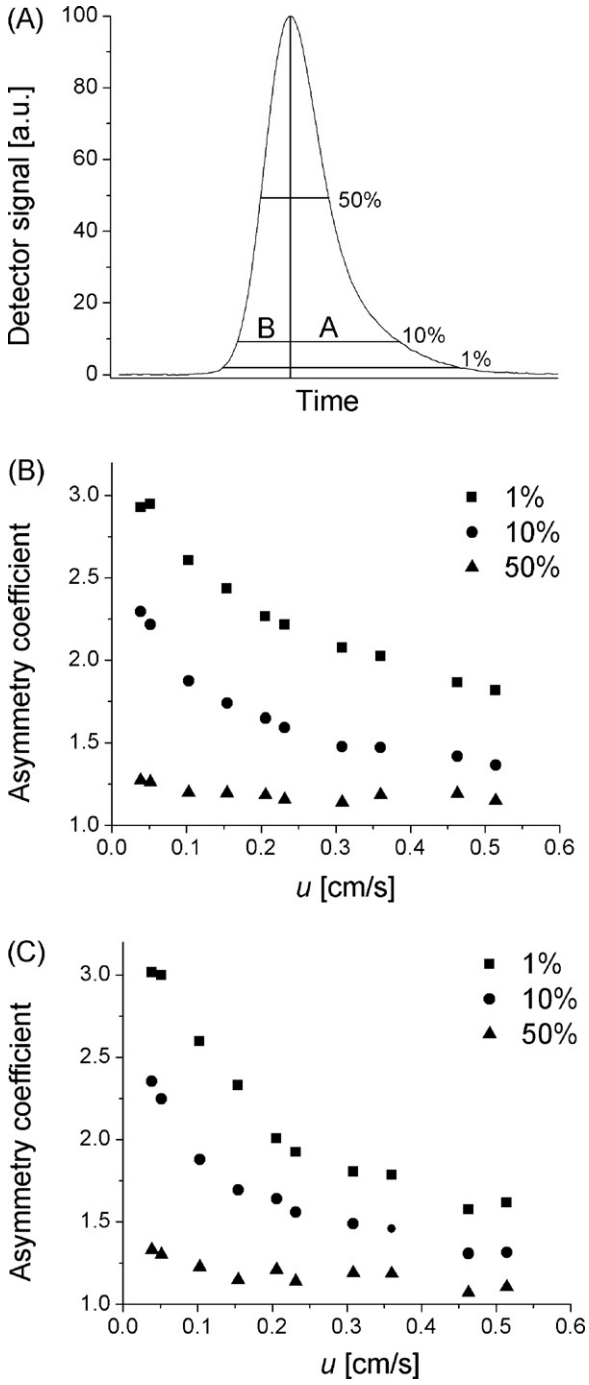

Fig. 5. Determination of asymmetry coefficient (B/A) (A) and asymmetry coefficients of L-Ala-L-Ala (B) and D-Ala-D-Ala (C) as a function of linear flow velocity. Mobile phase: 5 mM H_2SO_4 in methanol–water (70:30, v/v).

where the constant C' includes only contributions of the intraparticle diffusion and adsorption kinetics and the external mass transfer term is

$$H_{ext} = uf_1\delta_{ext} \tag{20}$$

with

$$f_1 = 2\left(\frac{k_1}{1+k_1}\right)^2 \tag{21}$$

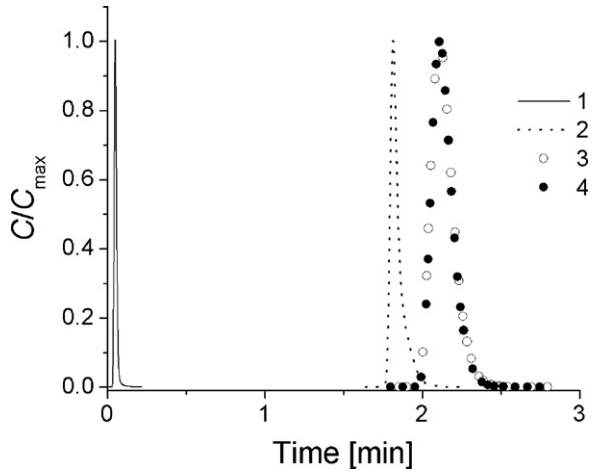

Fig. 6. Chromatograms of toluene recorded in system without column (1), with column (2), with a capillary (270 μl) installed before (3) or after (4) the column. Sample volume 2 μl, toluene concentration 0.5 g/l. Mobile phase: 5 mM H_2SO_4 in methanol–water (90:10, v/v).

H_{ext} and C' are equal to zero for a non-retained tracer. Then the plate height is determined only by the axial dispersion:

$$H - H_{ext} = H = A'(u) + \frac{2\gamma D_m}{u} \quad (22)$$

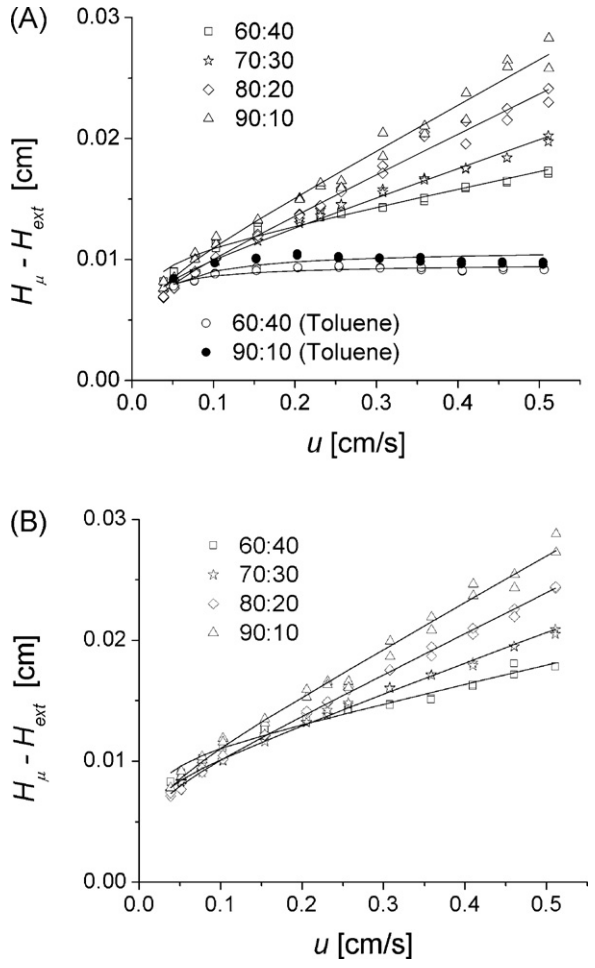

Fig. 7. Plots of HETP (moment method) corrected for the external mass transfer contribution as a function of the linear flow velocity for L-Ala-L-Ala and toluene (A) and D-Ala-D-Ala (B) at different mobile phase compositions. Symbols represent the experimental data, lines show approximations by Eq. (19).

Table 1
Best-fit parameters of the plate height equation[a,b]: toluene.

Coefficient	Methanol–water ratio	
	60:40	90:10
ω_4	20.85	21.60
λ_4	8.83	10.05

[a] Derived from H_μ values.
[b] Regression standard deviation reduced to the lowest and highest HETP value was not worse than 6.5 and 5.0%, respectively.

Below we consider dependencies of the HETP on the linear velocity, so called van Deemter plots, for a non-retained tracer (toluene) and for the optical isomers of Ala-Ala.

4.2.2.1. Toluene. Band broadening of toluene peaks is controlled by the Giddings terms. Fig. 7 shows that the HETP is constant at high flow rates as expected and decreases for $u < 0.2$ cm/s (Fig. 7). Thus the influence of molecular diffusion term is negligible within a range of flow rates studied. The H_μ *vs.* u graphs for different concentrations of methanol in the mobile phase are reasonably close to each other. The absolute coincidence is not expected as axial dispersion depends on solvent viscosity to a degree and this latter is a function of methanol content. Besides the profile of the injection perturbation is somewhat different for different mobile phase compositions. As it was mentioned above, toluene migrates through the column along with this perturbation. Thus, its profile will respond to this circumstance too. It is difficult to evaluate the extent of the effect in question. Noticing that the Van Deemter plots for toluene and for the Ala-Ala enantiomers are in a good agreement at low u as theory predicts, one can suppose that the influence of the inject perturbation is not intense. The experimental data can be approximated with Eq. (22) using the Giddings' estimation for the trans-channel, short-range inter-channel, and long-range inter-channel eddy dispersion and adjustable parameters ω_4 and λ_4. For the obstructive factor γ, we adopted value 0.65 from a work of Khirevich et al. [24]. Other authors reported similar values for γ [25,50]. The best fit parameters given in Table 1 will be discussed in the next section in comparison with data for Ala-Ala.

4.2.2.2. Alanyl-alanine. Van Deemter plots in the corrected HETP–u coordinates are shown in Figs. 7 and 8. The plots for different mobile phase compositions converge at low flow velocities and diverge as u increases, clearly showing importance of adsorption kinetics in band broadening. This tendency holds true both for H_μ and for $H_{0.5}$ quantities. The plots for the "second moment" HETP (Fig. 7) are visibly curved, concave downwards at $u < 0.25$ cm/s for eluents with 60 and 70% of methanol. The curvature is diminishing as the mobile phase becomes less aqueous. On the contrary, the graphs for the "half height" HETP apparently display a typical van Deemter behaviour, even a tendency to the minimum at low flow velocity (owing to the molecular diffusion term) can be recognized. It proves that the peculiarity of $H_\mu(u)$ curves results from tailing of peaks. It supports the hypothesis that some axial dispersion mechanism contributes to tail formation to a degree. To avoid a redundant superimposition of data on graphs, the data are presented separately for the LL- and DD-enantiomers. Should the curves be plotted together, one could see that those coincide at a low flow rate and slightly converge at a high flow rate, degree of convergence reducing as the water content in the mobile phase decreases. This was expected because when u approaches zero, the axial dispersion, which is an achiral phenomenon, is becoming important whereas the contribution of the enantioselective adsorption kinetics is becoming negligible.

Table 2 lists the best fitting parameters of Eq. (19) determined both for the H_μ and $H_{0.5}$ data. Note that only characteristics of

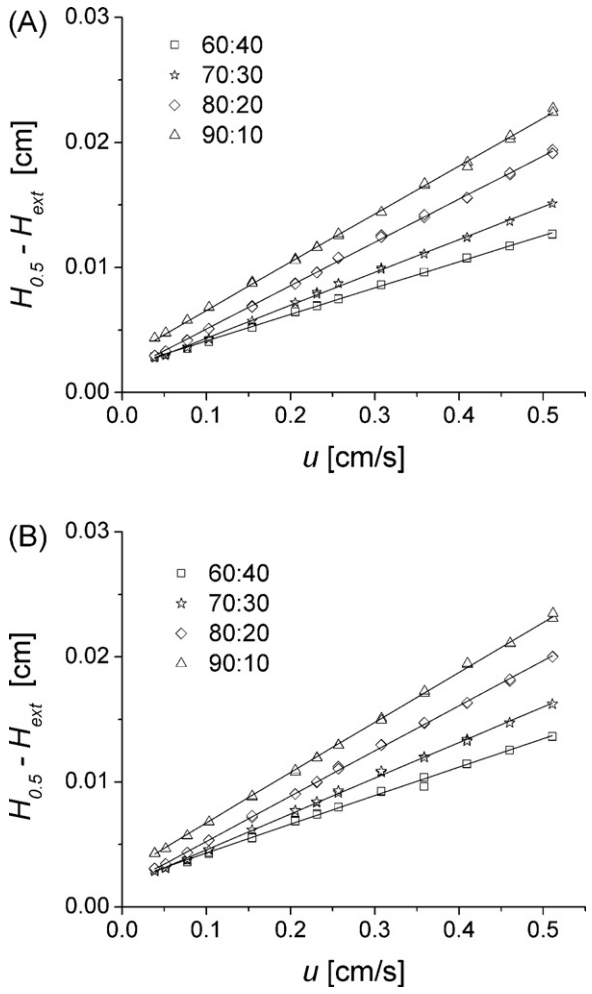

Fig. 8. Plots of HETP (half-height method) corrected for the external mass transfer contribution as a function of the linear flow velocity for L-Ala-L-Ala (A) and D-Ala-D-Ala (B) at different mobile phase compositions. Symbols represent the experimental data, lines show approximations by Eq. (19).

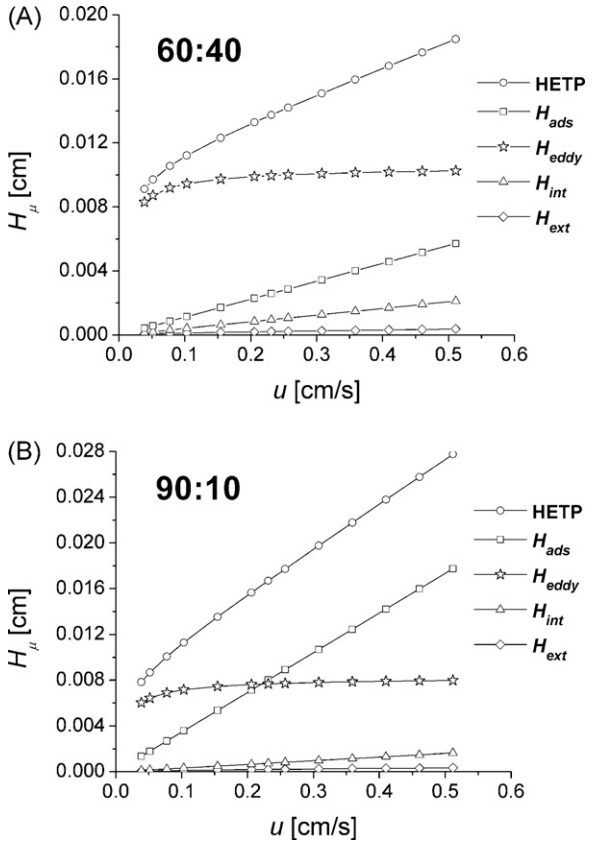

Fig. 9. HETP (moment method) of D-Ala-D-Ala and its contributions as a function of the linear flow velocity for mobile phase with 60 (A) and 90% of methanol (B). Legend symbols H_{ads}, H_{eddy}, H_{int}, and H_{ext} designate the contributions to the HETP from adsorption kinetics, eddy dispersion, the intraparticle mass transfer, and the external mass transfer, respectively. Note that the contribution of longitudinal molecular diffusion is not plotted since it is negligible.

the trans-column eddy dispersion (ω_4, λ_4) and adsorption kinetics were evaluated whereas those of the external and intraparticle mass transfer were obtained from semi-empirical correlations as described above. The longitudinal molecular diffusion was taken into account with the obstructive factor $\gamma = 0.65$ [24]. Giddings' estimation for the eddy dispersion parameters ω_i and λ_i for $i = 1$, 2, 3 were used in the calculations. In all the cases agreement between the best fit curves and the experimental data was good (Figs. 7 and 8). First, let us analyse the set of coefficients derived from H_μ values. The ω_4 coefficient relating to the diffusion transfer mechanism in the Giddings coupling theory of eddy dispersion [22] fluctuates around the value of 20 as the methanol–water ratio changes. This figure is roughly agrees with the estimation given by Gritti and Guiochon ([25]; see Section 2). The flow transfer parameter λ_4 seems to be a parabola-like function of the mobile phase composition. On the average, it differs almost by an order of magnitude from the estimation of the above authors. The fact of correlation between the parameter of question and mobile phase content can be ascribed to the dependence of the flow velocity profile on viscosity of the mobile phase, which changes approximately by 40% over a range of solvent compositions studied. Considering the data for toluene one can find that the structure parameter ω_4 is close to a respective characteristic measured with the dipeptide. Agreement is somewhat worse for the λ_4 value that can be explained by the experimental error.

Table 2
Best-fit parameters of the plate height equation[a]: alanyl-alanine.

Coefficient	Method	Methanol–water ratio			
		60:40	70:30	80:20	90:10
ω_4	H_μ	20.9	20.0	19.9	20.7
ω_4	$H_{0.5}$	20.87	20.87	20.87	20.87
λ_4	H_μ	9.6	7.5	6.7	7.5
λ_4	$H_{0.5}$	1.46	1.15	1.06	2.25
C (LL), s	H_μ	0.0140	0.0235	0.0328	0.0371
C (LL), s	$H_{0.5}$	0.0206	0.0259	0.0342	0.0380
C (DD), s	H_μ	0.0154	0.0249	0.0333	0.0379
C (DD), s	$H_{0.5}$	0.0224	0.0282	0.0358	0.0396
k_{ads} (LL), 1/s	H_μ	22.3	14.7	14.4	16.6
k_{ads} (LL), 1/s	$H_{0.5}$	13.5	13.1	13.7	16.2
k_{ads} (DD), 1/s	H_μ	26.9	18.1	17.6	19.3
k_{ads} (DD), 1/s	$H_{0.5}$	16.6	15.7	16.2	18.4

[a] Regression standard deviation reduced to the lowest and highest HETP value was not worse than 10 and 2.6%, respectively.

Figs. 9 and 10 compare contributions of different dispersion mechanisms to the band broadening. Only plots for the 60 and 90% methanol mobile phases are shown. Those for the solvents with 70 and 80% of methanol showing intermediate results are omitted for the sake of brevity. Consider at first the graphs for the H_μ values. It is seen that according to the GR model the curvature of the van Deemter plots is explained by the eddy dispersion. The respective term greatly prevails the rest band-broadening contributions for the (60:40) methanol–water mobile phase. It is still considerable,

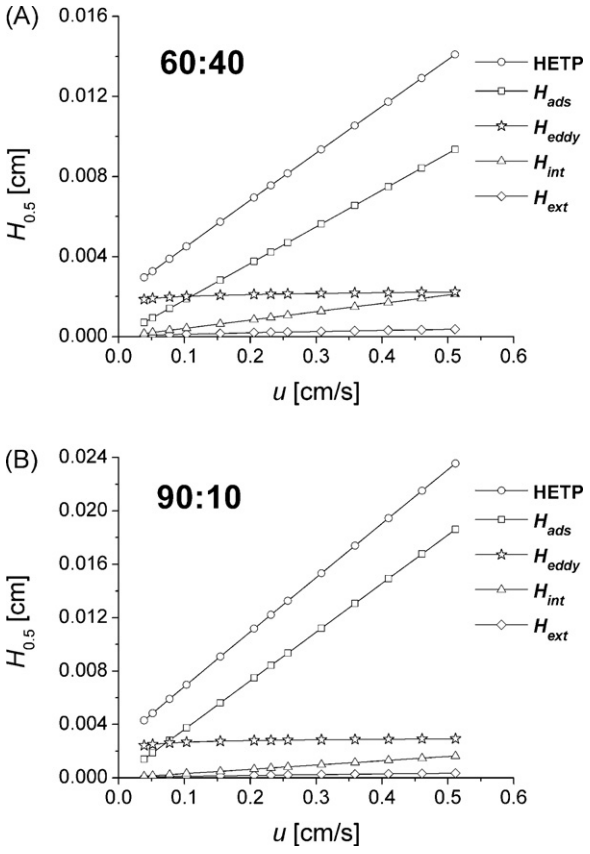

Fig. 10. HETP (half-height method) of D-Ala-D-Ala and its contributions as a function of the linear flow velocity for mobile phase with 60 (A) and 90% of methanol (B). Same symbols as in Fig. 9.

yet already comparable with the adsorption kinetics part at 90% of methanol. An absolute value of the H_{eddy} term changes moderately as a function of eluent composition, 90% of this quantity resulting from the trans-column effect. The main factor causing a decline of a relative importance of the eddy dispersion term is an increase of the adsorption rate constants (Table 2) as the percentage of water in the mobile phase decreases. A picture similar to one shown in Fig. 9b was observed for the naproxen enantiomers on another brush-type CSP Whelk-O1 (Pirkle-type selector) [14] although the effect was less pronounced. The effect of the eddy dispersion turns out to be minor in a structure of the $H_{0.5}$ value (Fig. 10). In this case, the *C*-term is predominant within almost the entire range of flow rates studied. Comparison of the sets of the plate equation parameters shows that the only principal difference between the half-height and second moment HETP is in the λ_4 coefficient, which is considerably smaller in the former case. In fact, such a λ value conditions the magnitude of the H_{tcol} contribution to the broadening of half-height width to be $\sim 3d_p$ that is common for well-packed 5 μm particle HPLC columns [25,50]. It is logical then to suppose that an observed large peak tailing is due to the trans-column eddy dispersion.

The value of the intraparticle diffusion term ($f_1\delta_{\text{int}}$) evaluated by the Mackie and Mears model is by factor 3.7 (60% of methanol) to 12 (90% of methanol) less than the C' coefficient. It suggests an important role of kinetics of adsorption/desorption proper. It is not common in the studies of column efficiency in chiral chromatography. On the contrary, Da Silva et al. [51] reported a fast adsorption for the bupivacain enantiomers on Kromasil CHI-TBB CSP, Asnin et al. [14] observed a minor influence of adsorption kinetics comparing to the intraparticle diffusion resistance to the mass transfer for naproxen on Whelk-O1. Miyabe and Guiochon [52] came to the same conclusion studying the adsorption dynamics of phenylalanine on a MIP CSP. As an example of opposite, microcrystalline cellulose triacetate (MCTA) microbeads are to be given. Adsorption rate constant of (*S*)-Tröger's base on this adsorbent from ethanol was found to be $\sim 0.5\ s^{-1}$ [53]. The value of k_{ads} determined in the given study is much higher (Table 2). It is also by two orders of magnitude larger than the overall mass transfer coefficient for the ketamine enantiomers or the praziquantel enantiomers on MCTA from ethanol [9] or methanol [6], respectively. Difference between the adsorption rates of the optical antipodes on ChiroSil RCA is low and the column efficiency is approximately the same for both enantiomers. Taking into account previous results [14,48] one can suppose that this feature is peculiar to brush-type CSPs as contrary to MCTA. The adsorption rate constant negatively correlates with the equilibrium coefficient, which is explainable provided that the inclusion is an activated process. Then a lower affinity would attribute to a smaller activation barrier. Note that the ratio $k_{ads}(D)/k_{ads}(L)$ decreases approaching 1 as the methanol percentage (hence, the retention factor) increases. At the same time, selectivity does not change significantly, remaining ~1.3.

4.3. Conclusion

The retention of Ala-Ala on the ChiroSil RCA stationary phase is enantioselective both in terms of adsorption equilibrium and adsorption kinetics. The retention factor of Ala-Ala enantiomers increases with growth of methanol content in the mobile phase that is in a correlation with a decrease of solute solubility. The k' value is also a function of the column pressure that only partially can be explained by thermodynamics (dependence of the equilibrium constant on pressure). The magnitude of pressure induced variations does not exceed 12%.

A distinctive feature of the studied column is a significant peak tailing at low flow rates. This phenomenon was found to result from the eddy dispersion or, more precisely, from the contribution associated with flow velocity inequalities on the trans-column scale. This finding is surprising because usually peak tailing is explained by a slow or heterogeneous adsorption-desorption kinetics. In the given case the kinetic resistance to mass transfer contributes appreciably to the band broadening of the upper part of peaks (the zone of high solute concentration) whereas its influence on the tailing seems to be minor or masked by large axial dispersion. The magnitude of the kinetic contribution positively correlates with the retention of a solute.

A large eddy diffusion associated with peak tailing explains a relatively low efficiency of the column in study. For commonly used flow rates (~0.3 cm/s), the respective plate equation term varies within a range of $(12–18)d_p$ depending on mobile phase composition. Similar or even higher figures were reported for columns packed with MCTA or silica coated with chemically modified cellulose [7–9]. However this is unusual for other types of CSPs [51,52] including brush-type adsorbents [14], in which case the axial dispersion contribution was close to the theoretical limit of $2d_p$. A similar value of an apparent axial dispersion term for the ChiroSil RCA column was derived from the peak width at half-height. It suggests that once conditions stipulating the peak tailing are eliminated, the column could demonstrate a higher efficiency.

The data presented are in line with the hypothesis that the mass transfer properties of a ChiroSil RCA CSP are intermediate between the properties of bulk polysaccharides like MCTA with poor mass transfer kinetics and those of high efficient Pirkle-type CSPs. It results from a dual nature of crown ether-based adsorbents. On the one hand, those adsorb by a relatively slow inclusion mechanism. On the other hand, such (brush-type) stationary phases provide an easy access to chiral selectors for solutes. A further accumulation of information is necessary to draw solid conclusions.

Acknowledgement

The authors thank Prof. Georges Guiochon (University of Tennessee, Knoxville) for interest to our work and valuable comments. We also thank Dr. Fabrice Gritti (University of Tennessee, Knoxville) for fruitful discussion and his advice to use toluene as a non-retained tracer. This work was supported by a grant from the Next-Generation BioGreen 21 program (SSAC 2011), Rural Development Administration, Republic of Korea.

References

[1] M. Lämmerhofer, J. Chromatogr. A 1217 (2010) 814.
[2] E. Francotte, in: E. Francotte, W. Lindner (Eds.), Chirality in Drug Research, Wiley–VCH, Weinheim, 2006, p. 155.
[3] W.A. König, D.H. Hochmuth, J. Chromatogr. Sci. 42 (2004) 423.
[4] I. Marle, S. Jönsson, R. Isaksson, C. Pettersson, G. Pettersson, J. Chromatogr. 648 (1993) 333.
[5] T. Fornstedt, G. Zhong, Z. Bensetiti, G. Guiochon, Anal. Chem. 68 (1996) 2370.
[6] B.-G. Lim, Ch.-B. Ching, Ind. Eng. Chem. Res. 35 (1996) 169.
[7] A.M. Rizzi, J. Chromatogr. 478 (1989) 71.
[8] C.V. Goncalves, M.J.S. Carpes, C.R.D. Correa, C.C. Santana, Chem. Eng. J. 133 (2007) 151.
[9] I. Da Silva, M.A.G. dos Santos, V. De Veredas, C.C. Santana, Sep. Purif. Technol. 43 (2005) 103.
[10] T. O'Brien, L. Crocker, R. Thompson, K. Thompson, P.H. Toma, D.A. Conlon, B. Feibush, C. Moeder, G. Bicker, N. Grinberg, Anal. Chem. 69 (1997) 1999.
[11] H. Kim, K. Kaczmarski, G. Guiochon, Chem. Eng. Sci. 60 (2005) 5425.
[12] P. Sajonz, M. Kele, G. Zhong, B. Sellergren, G. Guiochon, J. Chromatogr. A 810 (1998) 1.
[13] Y. Chen, M. Kele, I. Quiñones, B. Sellergren, G. Guiochon, J. Chromatogr. A 927 (2001) 1.
[14] L. Asnin, K. Horvath, G. Guiochon, J. Chromatogr. A 1217 (2010) 1320.
[15] M. Bechtold, A. Felinger, M. Held, S. Panke, J. Chromatogr. A 1154 (2007) 277.
[16] M.C. Ringo, Ch. E. Evans, Anal. Chem. 69 (1997) 4964.
[17] E. Bang, J.-W. Jung, W. Lee, D.W. Lee, W. Lee, J. Chem. Soc., Perkin Trans. 2 (2001) 1685.
[18] M.H. Hyun, J. Sep. Sci. 26 (2003) 242.
[19] U. Conrad, B. Chankvetadze, G.K.E. Scriba, J. Sep. Sci. 28 (2005) 2275.
[20] G. Guiochon, A. Felinger, A.M. Katti, S.G. Shirazi, Fundamentals of Preparative and Nonlinear Chromatography, Second ed., Academic Press, Boston, MA, 2006.
[21] A. Felinger, J. Chromatogr. A 1126 (2006) 120.
[22] J. Giddings, Dynamics of Chromatography. Principles and Theory, Marcel Dekker, New York, 1965.
[23] F. Gritti, G. Guiochon, Anal. Chem. 78 (2006) 5329.
[24] S. Khirevich, A. Höltzel, A. Seidel-Morgenstern, U. Tallarek, Anal. Chem. 81 (2009) 7057.
[25] F. Gritti, G. Guiochon, AIChE J. 56 (2011) 1495.
[26] J.J.V. Deemter, F.J. Zuiderweg, A. Klinkenberg, Chem. Eng. Sci. 5 (1956) 271.
[27] E.J. Wilson, C.J. Geankoplis, Ind. Eng. Chem. Res. (Fundam.) 5 (1966) 9.
[28] K. Miyabe, M. Ando, N. Ando, G. Guiochon, J. Chromatogr. A 1210 (2008) 60.
[29] J.S. Mackie, P. Meares, Proc. R. Soc. (Lond.) A232 (1955) 498.
[30] B. Poling, J. Prausnitz, J. O'Connell, The Properties of Gases and Liquids, 5th ed., McGraw-Hill, New York, 2001.
[31] J. Billen, K. Broeckhoven, A. Liekens, K.N. Choikhet, G. Rozing, G. Desmet, J. Chromatogr. A 1210 (2008) 30.
[32] T. Fornstedt, P. Sajonz, G. Guiochon, Chirality 10 (1998) 375.
[33] L. Asnin, K. Sharma, C. Upadhyaya, S. Park, Bull. Kor. Chem. Soc. (submitted for publication).
[34] S. Jacobson, S. Golshan-Shirazi, G. Guiochon, J. Am. Chem. Soc. 112 (1990) 6492.
[35] T. Fornstedt, P. Sajonz, G. Guiochon, J. Am. Chem. Soc. 119 (1997) 1254.
[36] B.-G. Lim, Ch.-B. Ching, R.B.H. Tan, Sep. Technol. 5 (1999) 213.
[37] H. Yamazaki, J. Chromatogr. 27 (1967) 14.
[38] T. Fornstedt, G. Zhong, G. Guiochon, J. Chromatogr. A 741 (1996) 1.
[39] G. Gotmar, T. Fornstedt, G. Guiochon, J. Chromatogr. A 831 (1999) 17.
[40] J.H. Knox, R. Kaliszan, J. Chromatogr. 349 (1985) 211.
[41] A.L. Colmsjö, M.W. Ericsson, J. Chromatogr. 398 (1987) 63.
[42] J.V.H. Schudel, G. Guiochon, J. Chromatogr. 457 (1988) 1.
[43] F. Gritti, A. Felinger, G. Guiochon, J. Chromatogr. A 1136 (2006) 57.
[44] F. Gritti, G. Guiochon, J. Chromatogr. A 1206 (2008) 113.
[45] V.L. McGuffin, C.E. Evans, J. Microcol. Sep. 3 (1993) 513.
[46] P.W. Atkins, Physical Chemistry, W.H. Freeman, San Francisco, CA, 1978.
[47] X. Li, V.L. McGuffin, J. Liq. Chromatogr. Rel. Technol. 30 (2007) 965.
[48] L. Asnin, G. Götmar, G. Guiochon, J. Chromatogr. A 1091 (2005) 183.
[49] K. Miyabe, G. Guiochon, Anal. Chem. 83 (2011) 182.
[50] F. Gritti, G. Guiochon, AIChE J. 57 (2011) 333.
[51] I. Da Silva, V. De Veredas, M. Carpes, C. Santana, Adsorption 11 (2005) 123.
[52] K. Miyabe, G. Guiochon, Biotechnol. Prog. 16 (2000) 617.
[53] K. Miyabe, G. Guiochon, J. Chromatogr. A 849 (1999) 445.